Relationship between depth of a target in a turbid medium and fluorescence measured by a variable-aperture method

Liu Quan and Nirmala Ramanujam

Department of Biomedical Engineering, University of Wisconsin, Madison, Wisconsin 53706

Received July 27, 2001

The relationship between the depth of a target in a turbid medium and the fluorescence ratio profile measured by use of illumination and collection apertures with variable diameters and the same optical path is shown. The forward problem was studied by Monte Carlo simulations of the propagation of fluorescent light through a theoretical model of a biologically relevant system for a range of aperture diameters. The curve of the fluorescence ratio as a function of the aperture diameter is characterized by a maximum/minimum point whose position shifts linearly with the depth of the target. Furthermore, the position of the maximum/minimum is observed to be insensitive to variations in the fluorescence efficiency and to the optical properties of the target layer or the entire medium.

OCIS codes: 170.0170, 060.2350.

Fluorescence imaging in the ultraviolet–visible spectrum is ideally suited for detection of epithelial precancers and cancers[1] because the penetration depth of light in tissue falls on the same length scale (several hundred micrometers) as the tissue regions of interest.[2] Sources of contrast in the tissue include endogenous and (or) exogenous fluorophores.[1] Whereas fluorescence imaging provides spatial localization of neoplastic tissue, it provides little insight in the depth of the lesion. The depth of the lesion is a critical parameter in the staging of the disease and is routinely characterized in histological examination.[3] Depth localization of neoplasia in tissue with fluorescence imaging will enhance the diagnostic capability of this technique.

The relationship between the depth of a target (neoplastic layer) in a turbid medium (epithelial tissue) and the fluorescence ratio profile measured by use of illumination and collection apertures with variable diameters and the same optical path is discussed. We studied the forward problem by performing Monte Carlo simulations of fluorescent light propagation through a theoretical model of a biologically relevant system (containing endogenous or exogenous fluorescent targets) for a range of aperture diameters.

The theoretical model is based on a tissue culture system of squamous cell carcinoma (SCC),[4] which consists of a normal epithelium and an underlying extracellular matrix. The SCCs are inserted into the basal membrane of the epithelium. The SCCs first proliferate upward; after the entire epithelium is occupied, these cells will invade the basement membrane.[4] The SCCs can be transfected with molecular reporters such as Green Fluorescent Protein (GFP). This model has the potential broad use to represent all types of precancer and cancer of squamous epithelia, including those of the oral cavity, cervix, and skin.

Figure 1 shows a cross section of the theoretical model, which consists of three layers: the epithelial layer (thickness, $d_1 - d_2$); the SCC layer (thickness, d_2), which originates in the base of the epithelium; and the extracellular matrix (thickness, d_3). The thickness of the SCC layer was varied from zero to the full thickness of the epithelium (thickness, d_1) to signify the extent of proliferation upward. The thickness of the extracellular matrix was set to $d_3 = 2050\ \mu$m to represent an infinitely thick tissue. The lateral dimension of the model was assumed to be infinitely wide.

Table 1 summarizes the parameters of the model. The geometrical properties (thickness, $d_1 = 450\ \mu$m) and autofluorescence efficiency [at an excitation–emission wavelength pair (460, 520 nm)] were defined from the results of previous studies of human cervical tissue,[5] and we observed that the fluorescence efficiency of GFP-tagged SCCs (SCC–GFP) was 14 times higher than the autofluorescence of the SCCs. The optical properties and refractive indices were obtained from the literature.[2,6]

A weighted-photon Monte Carlo code[7] was modified to simulate fluorescence. We checked the accuracy of the code by comparing test simulation results with those reported in the literature.[8] We launched 10^7 photons in each simulation at random, uniformly distributed locations across the model surface over a range of angles defined by a numerical aperture of 0.37 and on a circular illumination area. We used a rejection scheme to determine whether an absorbed fraction of the photon packet was reemitted as a fluorescent photon. The fluorescence that escaped the medium was collected over an area and a numerical

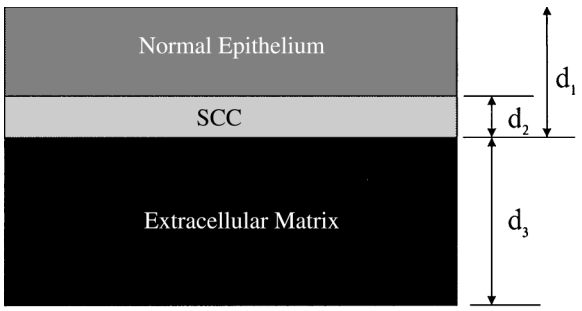

Fig. 1. Cross-sectional view of the theoretical model, which approximates the tissue culture system.

0146-9592/02/020104-03$15.00/0

Table 1. Parameters of the Theoretical Model[a]

Composition of Layer	Thickness of Layer (μm)	FE at $\lambda_{exc}-\lambda_{emm}$ Pair (460–520 nm)
Normal epithelium	d_1-d_2	0.2
SCC	d_2	0.05
SCC–GFP	d_2	0.7
Extracellular matrix	2050	0.6

[a]FE, fluorescence efficiency; μ_a, absorption coefficient; μ_s', reduced scattering coefficient; g, anisotropy; n, refractive index; λ_{exc}, excitation wavelength, λ_{emm}, emission wavelength. $d_1 = 450$ μm. μ_a, μ_s' (1/cm), g, and n, respectively, are at λ_{exc} (460 nm) 8.3, 6.62, 0.94, and 1.37 and at λ_{emm} (520 nm) 5.3, 6.02, 0.94, and 1.37 for simplicity without loss of accuracy.

aperture identical to those for the illumination (the illumination and collection areas overlapped completely). The refractive index of the medium above the model was set to be 1.452 to simulate an optical fiber, and that below the model was to 1.0. The radial and axial grid size was 0.0005 cm.

Figure 2 shows the normalized fluorescence ratio versus the illumination–collection aperture diameter for the model containing the SCC layer (without GFP) for three different depth/thickness values. Each of the curves represents the ratio of the fluorescence detected for a model that contains the SCC layer to that detected for a model without the SCC layer (i.e., SCC layer thickness, $d_2 = 0$). Each curve was interpolated and then normalized to unity. The aperture diameter that corresponds to the minimum point increases as the depth of the SCC layer increases (and its thickness decreases). Additionally, the curve broadens with increasing SCC layer depth.

Figure 3 displays the normalized fluorescence ratio versus aperture diameter for a model that contains the SCC–GFP layer for three different depth/thickness values and for variable optical properties at the excitation wavelength. Curves (1)–(3) indicate that there is a shift in the aperture diameter that corresponds to the maximum point with increasing SCC layer depth, as was shown in Fig. 2. We assessed the effect of changes in the absorption (μ_a) and the reduced scattering (μ_s') coefficients by independently varying μ_a and μ_s' at the excitation wavelength by $\pm 25\%$ for the SCC–GFP layer only [curves (4) and (5)] and for the entire model [curves (6) and (7)]. These simulations were carried out only for a depth/thickness ratio of 50 μm/400 μm, and the results are shown only for a 25% increase in the optical properties. The variation in μ_a results in a more pronounced effect on the profile than that in μ_s', as shown to the right of the maximum point. However, the position of the maximum point itself is relatively insensitive to changes in μ_a or μ_s'. The same conclusions were drawn from the results for a 25% decrease in optical properties (not shown).

Figure 4 displays the aperture diameter that corresponds to the minimum (for SCC) or maximum (for SCC–GFP) fluorescence ratio (MFR) versus the depth of the SCC layer. A fit to the SCC–GFP data indicates that there is a linear relationship between the MFR diameter and depth in the range 50–300 μm. Also, there is a similar relationship for the SCC (without GFP) data at depths of 50–200 μm. The slope of MFR diameter versus depth appears to be independent of the fluorescence efficiency, except at the sensitivity limit for SCC autofluorescence (>200 μm).

Figure 5 displays the MFR diameter versus depth of the SCC–GFP layer when both the depth and the thickness were varied (as in Fig. 3) and when only the depth was varied. When both depth and thickness were varied, the MFR diameter increased by 400 μm over a depth range of 100–300 μm. When only the depth was varied, the MFR diameter increased by 300 μm, over a depth range of 100–300 μm. Therefore the shift in MFR diameter depends primarily on the depth of the SCC layer. It should be noted that the percentage fluorescence contribution of the SCC layer to the total fluorescence detected is maximal at the MFR diameter.

This study demonstrates that the MFR diameter is related to the depth of an embedded target (neoplasia)

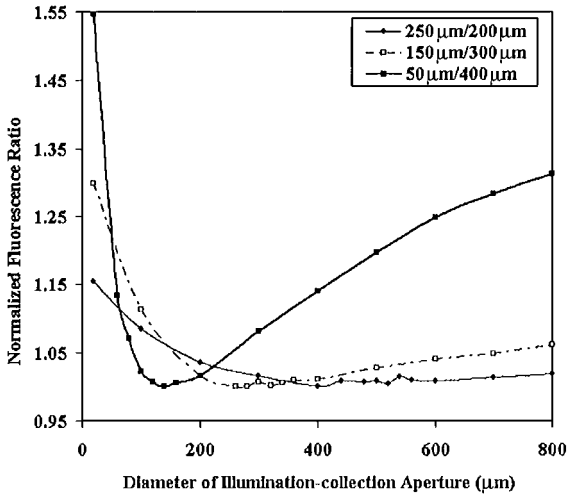

Fig. 2. Normalized fluorescence ratio versus diameter of the illumination–collection aperture for the model containing a SCC layer (without GFP).

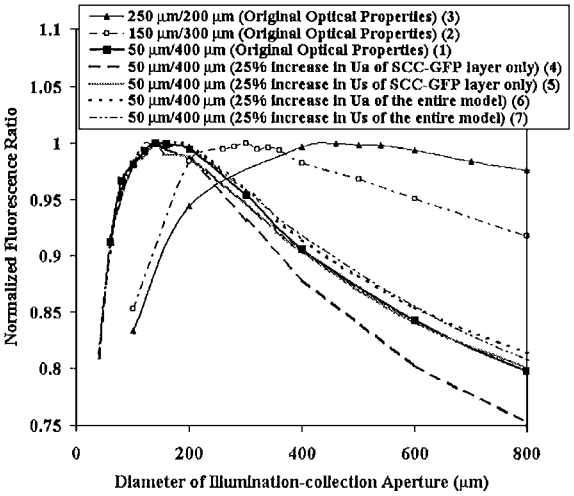

Fig. 3. Normalized fluorescence ratio versus aperture diameter for the model containing a SCC–GFP layer.

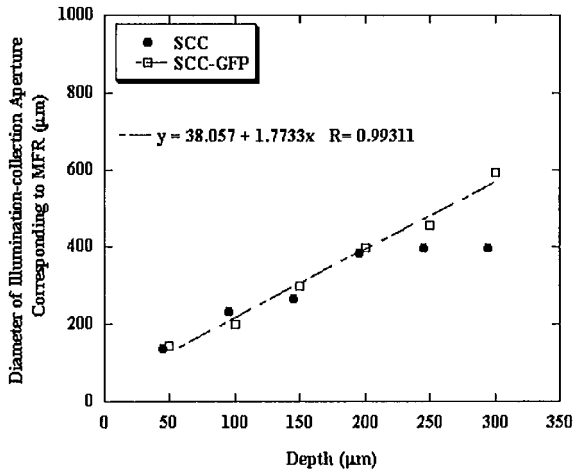

Fig. 4. Aperture diameter that corresponds to the minimum (for SCC) or the maximum (for SCC–GFP) fluorescence ratio (MFR diameter) verus to depth of the SCC layer.

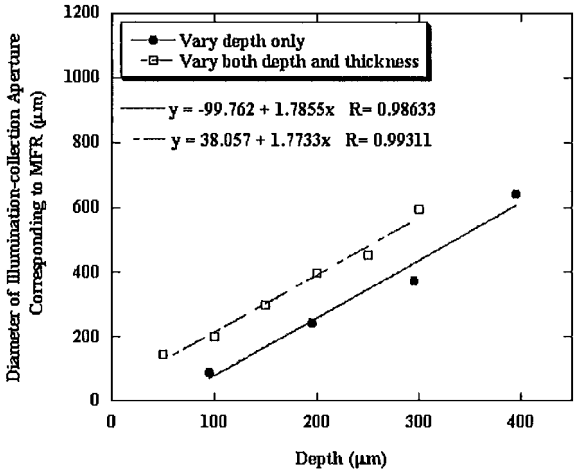

Fig. 5. MFR diameter relative to depth of the SCC–GFP layer when both the depth and the thickness were varied and when only the depth was varied.

in a turbid medium (epithelial tissue). In the short term, incorporating the variable-aperture method into *in vivo* fluorescence imaging strategies[9] could add another dimension of diagnostic information (depth) per pixel that is currently not available. The variable-aperture method could be incorporated by use of the fluorescence ratio at two aperture diameters[10] or by multivariate analysis of the entire profile to fully exploit the information content. In the long term, one could use this technique to perform quantitative depth localization with the MFR diameter. Although the results from this study indicate that the MFR diameter is relatively insensitive to variations in the optical properties of the target layer or of the entire model, a more careful evaluation of these effects will be carried out at both the excitation and emission wavelengths. Additionally, an inverse model or look-up table will be developed to relate the MFR diameter to the depth of the target in the turbid medium.

One can obtain a profile of the fluorescence ratio versus aperture diameter without significantly increasing the complexity of current fluorescence imaging systems. In principle, one can use a single optical fiber to detect the fluorescence per pixel. The aperture diameter can be varied by changing the distance between the fiber tip and the plane of the tissue surface. The feasibility of illuminating and collecting with the same fiber with sufficient signal-to-noise ratio will have to be evaluated, and it is expected to depend on the aperture diameters used and on the source of fluorescence contrast in the tissue system. An alternative approach to the single source–detector method proposed here is the multidistance approach,[10] which requires multiple sources and (or) detectors. The need for multiple sources and (or) detectors makes this approach more cumbersome than the variable-aperture method proposed here.

In summary, the variable-aperture method proposed in this Letter is ratiometric in nature and can be implemented in a stepwise manner as follows. First, depth-integrated fluorescence imaging can be used to localize the normal and abnormal tissue areas, as has been demonstrated with reasonably high accuracy.[9] Once the abnormality is localized, the variable-aperture method can be employed to yield the depth distribution of the fluorescence contrast in the abnormal tissue area.

N. Ramanujam's e-mail address is nimmi@engr.wisc.edu.

References

1. N. Ramanujam, Neoplasia **2,** 89 (2000).
2. G. I. Zonios, R. M. Cothren, J. T. Arendt, J. Wu, J. Van Dam, J. M. Crawford, R. Manoharan, and M. S. Feld, IEEE Trans. Biomed. Eng. **43,** 113 (1996).
3. R. S. Cotran, V. Kumar, and S. L. Robbins, *Robbins Pathologic Basis of Disease* (Saunders, Philadelphia, Pa., 1989), p. 34.
4. B. L. Allen-Hoffmann, S. J. Schlosser, C. A. Ivarie, C. A. Sattler, L. F. Meisner, and S. L. O'Connor, J. Invest. Dermatol. **114,** 444 (2000).
5. N. Ramanujam, R. Richards-Kortum, S. Thomsen, A. Mahadevan-Jansen, and M. Follen, Opt. Express **8,** 335 (2000), http://www.opticsexpress.org.
6. R. Marschesini, Lasers Surg. Med. **15,** 351 (1994).
7. L. Wang, S. L. Jacques, and L. Zheng, Comput. Methods Programs Biomed. **47,** 131 (1995).
8. A. J. Welch, C. Gardner, R. Richards-Kortum, E. Chan, G. Criswell, J. Pfefer, and S. Warren, Lasers Surg. Med. **21,** 166 (1997).
9. T. D. Wang, J. M. Crawford, M. S. Feld, Y. Wang, I. Itzkan, and J. Van Dam, Gastrointest. Endosc. **49,** 447 (1999).
10. T. H. Foster, E. L. Hull, M. G. Nichols, D. S. Rifkin, and N. Schwartz, Proc. SPIE **2979,** 741 (1997).